Asian Journal of Pharmaceutical Sciences 20 (2025) 101010

Available online at www.sciencedirect.com

ScienceDirect

journal homepage: www.elsevier.com/locate/AJPS

Research Article

All-stage targeted nanodiscs for glioma treatment by inducing cuproptosis and apoptosis of cancer cells and cancer stem cells

Yuan Ding[a], *Ruohan Chen*[a], *Jianfen Zhou*[a], *Yanning Bao*[a], *Nana Meng*[a], *Xudong Zheng*[a], *Shengmin Yang*[a], *Jiasheng Lu*[a], *Zhixuan Jiang*[a], *Yu Liu*[a], *Cao Xie*[a], *Linwei Lu*[b,c,*], *Weiyue Lu*[a,c,d,*]

[a] *School of Pharmacy, Fudan University & Key Laboratory of Smart Drug Delivery (Fudan University), Ministry of Education, Shanghai 201203, China*

[b] *Department of Integrative Medicine, Huashan Hospital, Fudan University, Shanghai 200040, China*

[c] *Institutes of Integrative Medicine, Fudan University, Shanghai 200032, China*

[d] *Shanghai Engineering Technology Research Center for Pharmaceutical Intelligent Equipment, and Shanghai Frontiers Science Center for Druggability of Cardiovascular non-coding RNA, Institute for Frontier Medical Technology, Shanghai University of Engineering Science, Shanghai 201620, China*

ARTICLE INFO

Article history:
Received 18 June 2024
Revised 21 October 2024
Accepted 5 November 2024
Available online 17 December 2024

Keywords:
Glioma
All-stage targeted therapy
Synergistic combination
Cancer stem cells
Ubiquitin-proteasome system
Cuproptosis

ABSTRACT

There remain several intractable challenges for chemotherapy in glioma treatment, including the blood-brain barrier (BBB), blood-brain tumor barrier (BBTB), and tumor heterogeneity caused by cancer stem cells (CSCs), which are resistant to conventional chemotherapy. Here, we established a nano strategy to kill glioma cells and CSCs, combining carfilzomib and bis(diethyldithiocarbamate)copper. The synergistic drug combination disturbed cell protein metabolism at different stages and induced apoptosis and cuproptosis. The Y-shaped targeting ligand pHA-VAP-modified nanodiscs were designed to help the chemotherapeutic agents cross the BBB/BBTB and finally accumulate in tumor site. This all-stage targeting and all-stage treatment nanomedicine significantly prolonged the survival in glioma-bearing mice and might inspire the rational design of advanced drug delivery platforms.

* Corresponding authors.
E-mail addresses: lw_lu@fudan.edu.cn (L. Lu), wylu@shmu.edu.cn (W. Lu).
Peer review under responsibility of Shenyang Pharmaceutical University.

https://doi.org/10.1016/j.ajps.2024.101010

1. Introduction

Glioma is the most common primary malignant brain tumor, which is an intractable disease with a poor prognosis [1,2]. There are several huge obstacles for nanomedicine treatment of glioma that are difficult to overcome. Firstly, it is widely recognized that the therapeutic approaches or diagnostic reagents are mostly limited by the blood-brain barrier (BBB) and blood-brain tumor barrier (BBTB) [3]. The BBB is a protective physiological barrier that is essential for securing specific substances, preventing the entry of macromolecules and unwanted cells [4]. It can be pathologically altered into the BBTB with phenotypic changes (low-grade glioma) and disrupted integrity (high-grade glioma) [4]. Although the BBTB has increased permeability compared to the intact BBB, it still retains some barrier functions [5]. Therefore, in glioma treatment, it is essential to firstly overcome the BBB in early tumor stages and in glioma cell infiltrated areas, and to secondly overcome the BBTB in the middle and advanced tumor stages, remaining effective treatment throughout the glioma progression. The next obstacle after crossing the BBB/BBTB is the high density of solid tumors that is difficult to be penetrated [6]. Crossing these barriers forms the basis for nanomedicines to function in glioma. The third ongoing obstacle is tumor heterogeneity. A crucial subpopulation with tumorigenic activity is named cancer stem cells (CSCs) or cancer stem-like cells, which underlies glioma initiation, evolution and drug resistance [7,8]. Accordingly, a combination of simultaneously eliminating glioma cells and CSCs is a potent treatment strategy for CSC-rooted heterogeneity.

It is known that the ubiquitin-proteasome system plays an important role in cell growth, development, morphogenesis and disease resistance, in which the poly-ubiquitylated (poly-Ub) proteins are cleaved by proteasomes [9]. Carfilzomib (CFZ) is a second-generation irreversible proteasome inhibitor, resulting in the accumulation of poly-Ub proteins and inducing apoptosis [10]. However, CFZ is not effective in solid tumors and the CSCs have shown drug resistance to CFZ [11,12]. Anti-alcohol abuse drug disulfiram (DSF) is a noticeable case for conventional drugs in new use when chelate with copper (Cu^{2+}) to form bis(diethyldithiocarbamate)copper (CuET), which can prolong the survival of cancer patients [13]. CuET inhibits the degradation of poly-Ub proteins by disabling another signaling pathway p97-nuclear protein localization homologue 4-ubiquitin fusion degradation 1 (p97-NPL4-UFD1) [13], and specifically inhibits CSCs growth [14,15]. Moreover, recent research has shown that CuET could induce a new type of cell death named cuproptosis by disturbing mitochondrial respiration [16]. Therefore, the combination of CFZ and CuET is probably a valid strategy to eliminate glioma cells and CSCs, inducing apoptosis and cuproptosis simultaneously. However, the poor solubility of CFZ and CuET is a major issue that limits their application *in vivo*.

Nanomedicines have been used to deliver the chemotherapeutics. The traditional drug delivery system liposomes show poor tumor permeability, while the lipid-based nanodiscs (NDs) can be prepared simply by changing the formulation of liposomes and can easily penetrate tumors because of their disc-like morphology [17–20]. Most nanomedicines have the passive-targeting ability based on the enhanced permeability and retention (EPR) effect. Since the EPR effect is not so robust in clinics or in orthotopic tumor models [21,22], nanomedicines should be based on an active-targeting strategy considering tumor vascular characteristics. In our previous research, a Y-shaped all-stage targeting ligand pHA-VAP (pV) was designed for glioma targeting [23,24], which was composed of BBB-crossing module p-hydroxybenzoic acid (pHA), targeting to dopamine receptor (DR) [25] and BBTB-crossing module stabilized peptide $^{D}S^{D}N^{D}T^{D}R^{D}V^{D}A^{D}P$ (VAP, targeting to glucose-regulated protein 78 (GRP78)) [26]. For the early glioma stage and glioma cell infiltrated areas, the BBB serves as the primary physiological barrier [25]. The pHA component can bind to DR on the BBB, enabling the nanomedicines to cross the BBB. For middle and advanced stages of glioma, the BBTB predominantly forms the barrier function [26]. VAP peptide in the pV targeting ligand can interact with GRP78, allowing the nanomedicines to cross this further developed barrier. After crossing these barriers, pV-modified nanomedicines can be taken up by both regular glioma cells and CSCs via receptor (GRP78 and DR) mediated endocytosis. Therefore, pV exhibits an integrated “all-stage targeting” effect, functioning in the entire tumor progression and targeting regular glioma cells and CSCs, dealing with the heterogeneity of the glioma.

Here, we prepared the pV-modified CFZ and CuET co-loaded NDs (pV-ND(CFZ/CuET)), proposing an all-stage targeting and synergistic treatment for glioma. CFZ and CuET were co-loaded in NDs by a two-step method at an optimized ratio, which was similar to cocktail therapy (Scheme 1A), and resulted in a strong synergistic effect both *in vitro* and *in vivo*. The pV-modified NDs showed a superior BBB/BBTB-crossing ability. More importantly, CFZ and CuET could eliminate both glioma cells and CSCs by disrupting the balance of ubiquitin-proteasome system and inducing apoptosis and cuproptosis (Scheme 1B). In orthotopic glioma models, pV-ND(CFZ/CuET) showed significantly higher accumulation in glioma and effectively prolonged the survival with good safety.

2. Materials and methods

2.1. Materials

1-palmitoyl-2-oleoyl-sn–glycero-3-phosphocholine (POPC), cholesterol (Chol) and N-(methoxyl polyethylene glycol 2000)−1,2-distearoyl-sn–glycero-3-phosphoethanolamine ($mPEG_{2000}$-DSPE) were obtained from AVT (Shanghai) Pharmaceutical Tech Co., Ltd. VAP ($^{D}S^{D}N^{D}T^{D}R^{D}V^{D}A^{D}P$)-SH, pHA-SH and pHA-VAP (pV)-SH were synthesized by GL Biochem, Ltd. (Shanghai, China). Mal-PEG_{3400}-DSPE and NH_2-$mPEG_{3400}$-DSPE were purchased from Laysan Bio Inc. (Arab, AL). Methylthiazolyldiphenyl-tetrazolium bromide (MTT), cell counting kit-8 (CCK-8), collagenase II, carfilzomib (CFZ), 1,1′-dioctadecyl-3,3,3′,3′-tetramethylindotricarbocyanine (DiR), chlorpropamide (Chlo), fluorescein isothiocyanate (FITC) and AnnexinV-FITC/PI apoptosis assay kit were purchased from Meilun Biotechnology Ltd. Co. (Dalian,

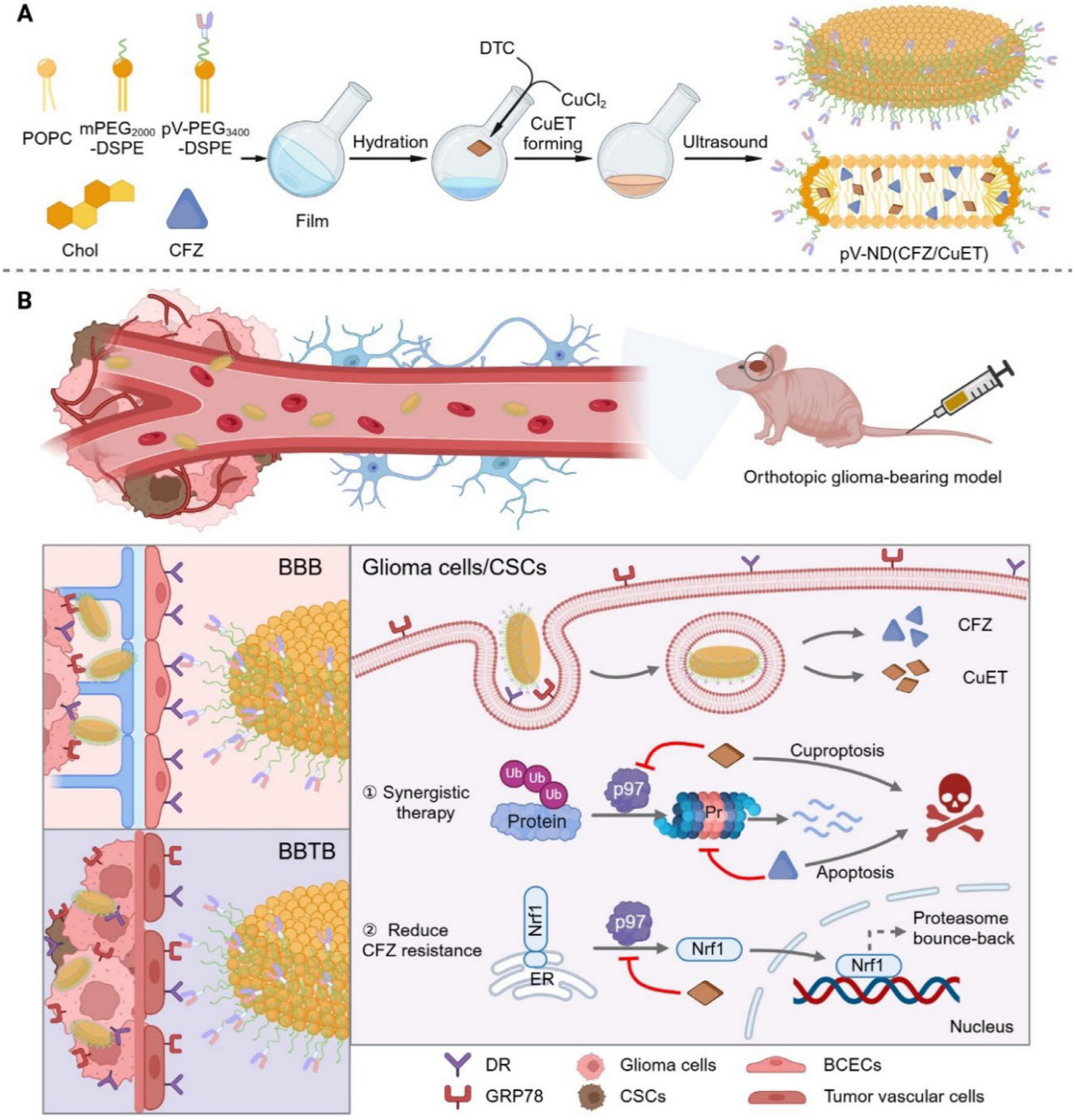

Scheme 1 – Schematic diagram of pV-ND(CFZ/CuET) preparation and its all-stage targeting and treatment for glioma. (A) pV-ND(CFZ/CuET) was prepared by thin-film hydration with a two-step drug-loading method. (B) The Y-shaped targeting ligand pV endowed NDs with the BBB/BBTB-crossing ability. The disc-like NDs delivered CFZ and CuET simultaneously into glioma. The released CFZ and CuET synergistically disrupted the balance of ubiquitin-proteasome system and induced apoptosis and cuproptosis, thereby exerting anti-glioma effects. Moreover, CuET could reduce CFZ resistance and inhibit CSCs specifically. This diagram was created with BioRender.

China). Sodium diethyldithiocarbamate trihydrate (DTC) was supplied by Shanghai Aladdin Biochemical Technology Co., Ltd. Copper chloride dihydrate ($CuCl_2$), trifluoroacetic acid (TFA), dimethyl sulfoxide D_6 (DMSO-D_6), collagenase IV and DNase I were obtained from Sigma-Aldrich (St. Louis, MO). Ammonium tetrathiomolybdate (VI) (TTM), Boc-Asp(OMe)-fluoromethyl ketone (Boc-D-FMK), NG-Nitroarginine methyl ester hydrochloride (L-NAME), N-Acetylcysteine (NAC), necrostatin-1 (Nec-1), ferrostatin-1 (Fer-1) and pepstatin A were purchased from MedChemExpress (Monmouth Junction, NJ, USA). Giemsa staining solution, sodium potassium ATPase antibody (AF1864) and β-actin antibody (AA128) were obtained from Beyotime Biotechnology (Shanghai, China). Dopamine Receptor D1 antibody (ab279713) was obtained from Abcam (Cambridge, USA). TCF11/NRF1 antibody (D5B10) and ubiquitin antibody (P4D1) were obtained from Cell Signaling Technology (Beverly, MA, USA). GRP78/Bip antibody (bsm-33224 M) was obtained from Bioss Antibodies (Woburn,

MA, USA). Other reagents were purchased from China National Pharmaceutical Group Corporation.

2.2. Cells and animals

Human glioma U87 cells were purchased from American Type Culture Collection (ATCC). Human umbilical vascular endothelial cells (HUVECs), mouse brain capillary endothelial cells (bEnd.3), human normal liver cells (HL7702) and human embryonic kidney 293 cells (HEK293) were purchased from Shanghai Institute of Biochemistry and Cell Biology, Chinese Academy of Sciences. Cells were cultured in Dulbecco's modified Eagle medium (DMEM) with 10 % fetal bovine serum (FBS) (Gibco) and 1 % penicillin-streptomycin (Gibco) at 37 °C under the humidified atmosphere containing 5 % CO_2. Rat primary brain capillary endothelial cells (BCECs) were cultured in EBM-2 MV SingleQuots medium (Lonza, Basel, Switzerland). Human glioma stem-like SHG66 cells were donated by the Department of Neurosurgery Laboratory at Huashan Hospital (Shanghai, China) and were cultured in serum-free medium (SFM) with 20 ng/ml of recombinant human basic fibroblast growth factor (bFGF, Thermo), 20 ng/ml of recombinant human epidermal growth factor (hEGF, Thermo), and 1×B27 (Thermo).

Male BALB/c nude mice and male ICR mice (20-22 g) were purchased from Shanghai Sippr-BK laboratory animal Co., Ltd. (Shanghai, China) and kept under specific pathogen-free (SPF) conditions. All the animal experiments were carried out in accordance with the guidelines evaluated and approved by the ethics committee of Fudan University.

2.3. Cytotoxicity assay and combination index (CI) analysis

U87 cells, SHG66 cells or HUVECs were seeded into 96-well plates (3,000 cells per well) and treated with a single drug or drug combination. After 72 h incubation, the cell viability of U87 cells and HUVECs was assessed by the MTT assay. Since SHG66 cells were non-adherent, the cell viability was assessed by CCK-8 kit. Non-linear regression analysis was performed using GraphPad Prism 9.5 to calculate IC_{50} values. The combination effect was assessed by the Chou-Talalay method [27,28], and the CI values were calculated by the CompuSyn software (https://www.combosyn.com/) according to the Eq. (1):

$$CI_X = D_A/(D_X)_A + D_B/(D_X)_B \quad (1)$$

where X represented the particular drug effect; $(Dx)_A$ and $(Dx)_B$ were the doses of drug A or B when causing the particular drug effect along; D_A and D_B were the doses of drug A and B when causing the particular drug effect together. CI < 1 indicated a synergistic effect; CI = 1 indicated an additive effect; CI > 1 indicated an antagonistic effect.

2.4. Preparation and characterization of NDs

2.4.1. Preparation of ND formulations

The targeting materials (pHA-PEG_{3400}-DSPE, VAP-PEG_{3400}-DSPE and pV-PEG_{3400}-DSPE) were synthesized by the reaction between sulfhydryl group (SH) in targeting ligands and maleimide group (Mal) in Mal-PEG_{3400}-DSPE. FITC-PEG_{3400}-DSPE was synthesized by the reaction between the amino group (NH_2) in NH_2-PEG_{3400}-DSPE and the isothiocyanate group in FITC. NDs were prepared using the thin film hydration method. 2.65 mg POPC, 1.56 mg Chol and 7 mg $mPEG_{2000}$-DSPE were dissolved in chloroform and then vacuumed to form a thin film. To prepare the targeting NDs, the molar ratio of targeting material was 2 %. The thin film was hydrated by 1 ml PBS (pH 7.4, 10 mM) and was granulated by probe sonication in an ice bath. CFZ and CuET (at a total amount of 1 mg) were loaded in two steps: CFZ was dissolved in chloroform and then vacuumed and hydrated. DSF and $CuCl_2$ were added into the resulting mixture successively to form CuET *in situ*. The mixture was then probe-sonicated in an ice bath. Besides, CuET was added directly into the chloroform at the same time with CFZ as control. The unloaded drug was removed by Sephadex G-50 size exclusion column. Preparation of fluorescent dye-loaded NDs was similar to that of drug-loaded NDs. 60 μg DiR or 2 % molar ratio of FITC-PEG_{3400}-DSPE was dissolved in chloroform together with POPC, Chol and $mPEG_{2000}$-DSPE. The following steps were the same as the above. Particle size and zeta potential of NDs were analyzed by ZS-10–82 Zetasizer (Malvern Instruments Ltd. Co., Malvern, UK).

2.4.2. Drug loading capacity, morphology and stability

Acetonitrile was added into NDs and the mixture was centrifuged. Then the supernatant was analyzed by HPLC. The encapsulation efficacy was calculated according to Eq. (2), and the drug loading efficacy was calculated according to Eq. (3):

$$\text{Encapsulation efficacy (\%)} = 100\% \times m_{loaded\ drug}/m_{added\ drug} \quad (2)$$

$$\text{Drug loading efficacy (\%)} = 100\% \times m_{loaded\ drug}/m_{total} \quad (3)$$

The morphology of ND(CFZ/CuET) and pV-ND(CFZ/CuET) was identified by cryo-electron microscopy (cyro-EM, Tecnai G2 F20 200 kV). The aspect ratios (ARs) of NDs were analyzed by Image J. Particle size was measured to evaluate ND stability at 4 °C in PBS or 37 °C in 50 % mouse serum.

2.4.3. In vitro drug release

Drug release was conducted by dialysis method in 10 mM PBS (pH 7.4 or 5.5) with 1.5 % SDS at 37 °C under 180 rpm shaking. 0.5 ml ND(CFZ/CuET) or pV-ND(CFZ/CuET) was added into a dialysis bag (100 kDa) and immersed into 15 ml release medium. 1 ml of release medium was withdrawn at each time point and replaced by an equal amount of fresh medium. Drug concentration was then analyzed by HPLC.

2.5. Colony formation assay and spheroid formation assay

For colony formation assay, U87 cells were seeded into 6-well plates (500 cells per well). After overnight culturing, pV-ND(CFZ) (CFZ 50 nM), pV-ND(CuET) (CuET 50 nM) or pV-ND(CFZ/CuET) (CFZ 50 nM and CuET 50 nM) was added for 3 h of incubation. Then the supernatant was replaced by drug-free culture medium and was refreshed every 3 d until

the colonies were visible. The colonies were fixed by cold methanol and stained with Giemsa reagent. Relative colony size was analyzed by Image J. For spheroid formation assay, SHG66 cells were digested into single cells by collagenase IV and seeded into 6-well plates (500 cells per well). After overnight culturing, pV-ND(CFZ) (CFZ 100 nM), pV-ND(CuET) (CuET 100 nM) or pV-ND(CFZ/CuET) (CFZ 100 nM and CuET 100 nM) was added for 3 h of incubation. The following steps were the same as the above.

2.6. Apoptosis assay

U87 or SHG66 cells were seeded into 6-well plates at a density of 1.8×10^5 cells/well. After overnight culturing, pV-ND(CFZ), pV-ND(CuET) or pV-ND(CFZ/CuET) was added for 48 h of incubation. U87 or SHG66 cells were digested into single cells and stained with Annexin V-FITC/PI for 15 min. Flow cytometry (CytoFLEX, Beckman, USA) was used to analyze the apoptotic cells, and apoptosis rates of cells were analyzed by FlowJo 10.8.1.

2.7. Cell rescue assay

Cell rescue assay was conducted according to a previous report [16]. Cell death-modulating compounds were added (at the concentrations as previously described) 6 h after seeding 3,000 cells per well in 96-well plates. After 16 h of incubation, the cell death-inducing NDs were added to induce cytotoxicity. Cell viability was measured 72 h after incubation.

2.8. Cellular uptake of NDs

U87 cells, HUVECs or bEnd.3 cells were seeded (1×10^5 cells per well) into 12-well plates. Primary BCECs were collected and seeded into 12-well plates with rat tail collagen. Cells were treated with FITC-labeled ND, pHA-ND, VAP-ND or pV-ND for 4 h Then the cells were collected and detected by flow cytometry and confocal laser scanning microscope (CLSM, Olympus SpinSR10, Japan).

2.9. Penetration of NDs into 3D U87 spheroids

The 3D U87 tumor spheroids were established according to a previous report [29]. The tumor spheroids were treated with FITC-labeled ND, pHA-ND, VAP-ND or pV-ND for 4 h and fixed with 4 % polyformaldehyde for 20 min. Then the spheroids were imaged by CLSM using Z-axis scanning mode.

2.10. In vitro BBB and BBTB transcytosis assay

For *in vitro* BBB model, SD rat primary BCECs were collected and seeded into the transwell upper chambers with rat tail collagen. Transendothelial electrical resistance (TEER) was detected, and the BCEC layer with TEER of over 300 $\Omega \cdot cm^2$ was used to assess the BBB-crossing ability. For *in vitro* BBTB model, HUVECs were seeded into the transwell upper chambers (1×10^4 cells per well) and U87 cells were seeded into the lower chambers (4×10^4 cells per well). After 3 d co-culturing, the upper chambers were transferred into a new 24-well plate. FITC-labeled ND, pHA-ND, VAP-ND or pV-ND were added into the upper chambers. The culture medium in the lower chambers was collected at each time point and replaced by an equal amount of fresh medium. The amount of NDs was analyzed by microplate reader (BioTek, USA). Furthermore, the monolayers of the BBB and BBTB models were fixed and imaged by CLSM.

2.11. Western blot

After different treatments, cells were washed and scraped in lysis buffer containing 1 % PMSF. Membrane protein extraction kit was used to collect membrane protein. Protein concentrations were quantified by bicinchoninic acid (BCA) assay. 20 μg protein was loaded and electrophoretically separated in the polyacrylamide gel, and then transferred onto a polyvinylidene difluoride membrane. The membrane was incubated with the corresponding primary antibodies overnight at 4 °C. Secondary antibody was then conjugated and the signals were visualized by adding chemiluminescence.

2.12. Pharmacokinetic study

Pharmacokinetic study was performed by using LCMS-8060 (Shimadzu, Japan). ND(CFZ/CuET) or pV-ND(CFZ/CuET) was administered via the tail vein of ICR mice (CFZ 2 mg/kg and CuET 1 mg/kg, molar ratio of 1:1). 50 μl of blood samples were collected at each time point from the retro-orbital plexus. The blood samples were centrifuged (4 °C, 1,100 g, 10 min) and 20 μl plasma was mixed with 80 μl cold acetonitrile (containing 10 ng Chlo). After centrifugation (4 °C, 15,000 g, 10 min), the drug concentration in the supernatant was quantified immediately. Data were acquired in product ion mode with Chlo [30] as the internal standard (positive ion mode, CFZ: 720.65>100.15 *m/z*; CuET: 361.20>116.20 *m/z*; Chlo: 277.25>111.15 *m/z*). The pharmacokinetic parameters were calculated by DAS 2.0.

2.13. In vivo targeting ability

The orthotopic U87 glioma model was established according to a previous method [23]. Briefly, male nude mice were anesthetized and 5×10^5 U87 cells were implanted into the striatum in the right brain. On 7 d after implantation, orthotopic glioma-bearing nude mice were intravenously administered with ND, pHA-ND, VAP-ND or pV-ND with DiR. Fluorescence images were captured with NIR imaging system (IVIS spectrum, PerkinElmer, Santa Clara, CA) at 2, 4, 8 and 12 h after administration. The fluorescence images of brains *ex vivo* were captured at 12 h after administration.

The CFZ/CuET amount in brain was also evaluated. Male nude mice bearing orthotopic glioma were intravenously administered with Free(CFZ/CuET), ND(CFZ/CuET), pHA-ND(CFZ/CuET), VAP-ND(CFZ/CuET) or pV-ND(CFZ/CuET) at a dosage of CFZ 2 mg/kg and CuET 1 mg/kg. After 2 and 12 h of administration, brains were harvested and immediately processed by homogenization in acetone at 4 °C, with Chlo as the internal standard. The mixture was centrifuged (4 °C, 15,000 g, 10 min) and the supernatant was kept at −80 °C for no longer than 6 h For LCMS-8060 analysis, the supernatant

was placed into a pre-cooled LC-sample rack and immediately analyzed.

2.14. Anti-orthotopic U87 glioma study

The orthotopic glioma model was established and the mice were randomly divided into eight groups on 7 d after implantation. Mice were intravenously administered with PBS, Free(CFZ/CuET), ND(CFZ/CuET), pHA-ND(CFZ/CuET), VAP-ND(CFZ/CuET), pV-ND(CFZ/CuET), pV-ND(CFZ) or pV-ND(CuET) at the dosage of CFZ 2 mg/kg and CuET 1 mg/kg every single injection on 7, 10, 13, 16 and 19 d after glioma modeling. On 20 d, mice were randomly selected and the organs were harvested for histological analysis (H&E staining) and immunostaining (CD133 and Nestin). Mice were weighed every other day, and their survival time was recorded every day and plotted as Kaplan-Meier survival curves.

Though Chou-Talalay method has been widely used to evaluate drug interactions *in vitro*, this multi-dose method requires a large number of subjects and is not suitable for costly animal experiments [27,28]. A q value method reported by JIN can directly use the original effects and the effects of two drugs do not have to be the same, so it can be used for animal experiments to preliminarily evaluate drug interactions [31]. q value was calculated according to Eq. (4):

$$q = E_{A+B}/(E_A + E_B - E_A \times E_B) \quad (4)$$

Where E_A and E_B were the effects of drug A and drug B separately; E_{A+B} was the effect of drug A and B in combination. For biological experiments, there was a margin of error of about 15 %. q between 0.85 and 1.15 indicated an additive effect; $q > 1.15$ indicated a synergistic effect; $q < 0.85$ indicated an antagonistic effect.

Since q value method has not been applied to the survival curve yet, we expanded its application to evaluate drug interactions on survival curves, taking median survival time (MST) extension rate as the E value into Eq. (4) to further calculate q value *in vivo* (Eq. (5)):

$$MST_{extension\ rate}(\%) = 100\% \times (MST_{treated} - MST_{control})/MST_{control} \quad (5)$$

where the $MST_{treated}$ was the MST of drug-treated group and the $MST_{control}$ was the MST of PBS group.

2.15. Statistical analysis

Data were presented as mean ± standard deviation (SD). Statistical significance was analyzed using GraphPad Prism 9.5, with unpaired Student's *t*-test for two-group comparison, one-way ANOVA followed by Tukey's comparison for multiple-group comparison, and log-rank test for median survival time, respectively. $P < 0.05$ was considered statistically significant ($^{*}P < 0.05$, $^{**}P < 0.01$, $^{***}P < 0.001$).

3. Results and discussion

3.1. Preparation and characterization of pV-ND(CFZ/CuET)

CuET could be synthesized by complexation between DTC and $CuCl_2$ at the molar ratio of 2:1. Compared with DTC, CuET showed the characteristic absorption peak at 435 nm (Fig. S1). The optimized molar ratio of CFZ/CuET was determined by MTT assay and CI value. The IC_{50} values decreased in step with the decrease of CFZ/CuET ratio (Fig. 1A and S2A&S2C). The CI values of U87 cells, SHG66 cells and HUVECs at Fa_{50} showed the lowest level at CFZ/CuET molar ratio of 1:1 (Fig. 1B and S2B&S2D). Besides, SHG66 cells showed natural resistance to CFZ with a much higher IC_{50} value (> 10 μM, Fig. S2A) than that of U87 cells (44.05 nM), while the IC_{50} value of CuET on SHG66 cells (193.64 nM) was close to that on U87 cells (141.91 nM). It was consistent with previous studies [14,15] that CuET could effectively inhibit CSCs.

NDs with no drugs were prepared by film-hydration method and the drug-loaded NDs were prepared in two steps. CFZ was dissolved in chloroform together with POPC, Chol and $mPEG_{2000}$-DSPE to form a film and then be hydrated. DSF and $CuCl_2$ were successively added into the hydration solution to form CuET *in situ* for a homogeneous system (Fig. S3A), otherwise CuET would precipitate when added in the rotary evaporation step (Fig. S3B), which was similar to that in PBS (Fig. S3C). The average particle sizes of ND(CFZ/CuET), pV-ND(CFZ/CuET), VAP-ND(CFZ/CuET) and pV-ND(CFZ/CuET) were around 100 nm, and their polydispersity index (PDI) were around 0.2 (Fig. 1C, Table S1). The zeta potential ranged from −13.9 mV to −10.5 mV due to the slight positive charge of the targeting ligands (Fig. 1D, Table S1). The drug loading capacity of the NDs ranged from 7.38 % to 7.76 % and the encapsulation efficiencies of CFZ or CuET were about 90 % (Fig. 1E, Table S2). The CFZ/CuET molar ratios of the NDs were around 1:1 (Fig. 1E, Table S2). Particle sizes of NDs remained stable for a month at 4 °C in PBS (Fig. S4A) and for 48 h at 37 °C in 50 % mouse serum (Fig. S4B). The release rate of CFZ was similar to that of CuET at pH 7.4 and pH 5.5 (Fig. 1F-1G). ND(CFZ/CuET) and pV-ND(CFZ/CuET) exhibited sustained release at pH 7.4 and released quickly at pH 5.5, mainly due to the enhanced solubility of CFZ and CuET in 1.5 % SDS at pH 5.5 (Fig. 1F-1G). Cryo-EM images of ND(CFZ/CuET) and pV-ND(CFZ/CuET) demonstrated the disc-like morphology of NDs, and the AR ratios of ND(CFZ/CuET) and pV-ND(CFZ/CuET) were 6.30 and 7.13, respectively (Fig. 1H).

3.2. Cytotoxicity and mechanisms of pV-ND(CFZ/CuET)

To analyze the growth inhibitory effect *in vitro*, cytotoxicity was examined on U87 cells, SHG66 cells and HUVECs. All the formulations inhibited cell growth in a dose-dependent manner (Fig. 2A-2C). Furthermore, bEnd.3 cells were chosen to mimic normal brain capillary endothelial cells to assess the safety of different formulations, which can be sub-cultured continuously. Different formulations showed less cytotoxicity on bEnd.3 cells (Fig. S5) when compared with that on U87 cells and HUVECs (Fig. 2A & 2C). The CI values of NDs showed

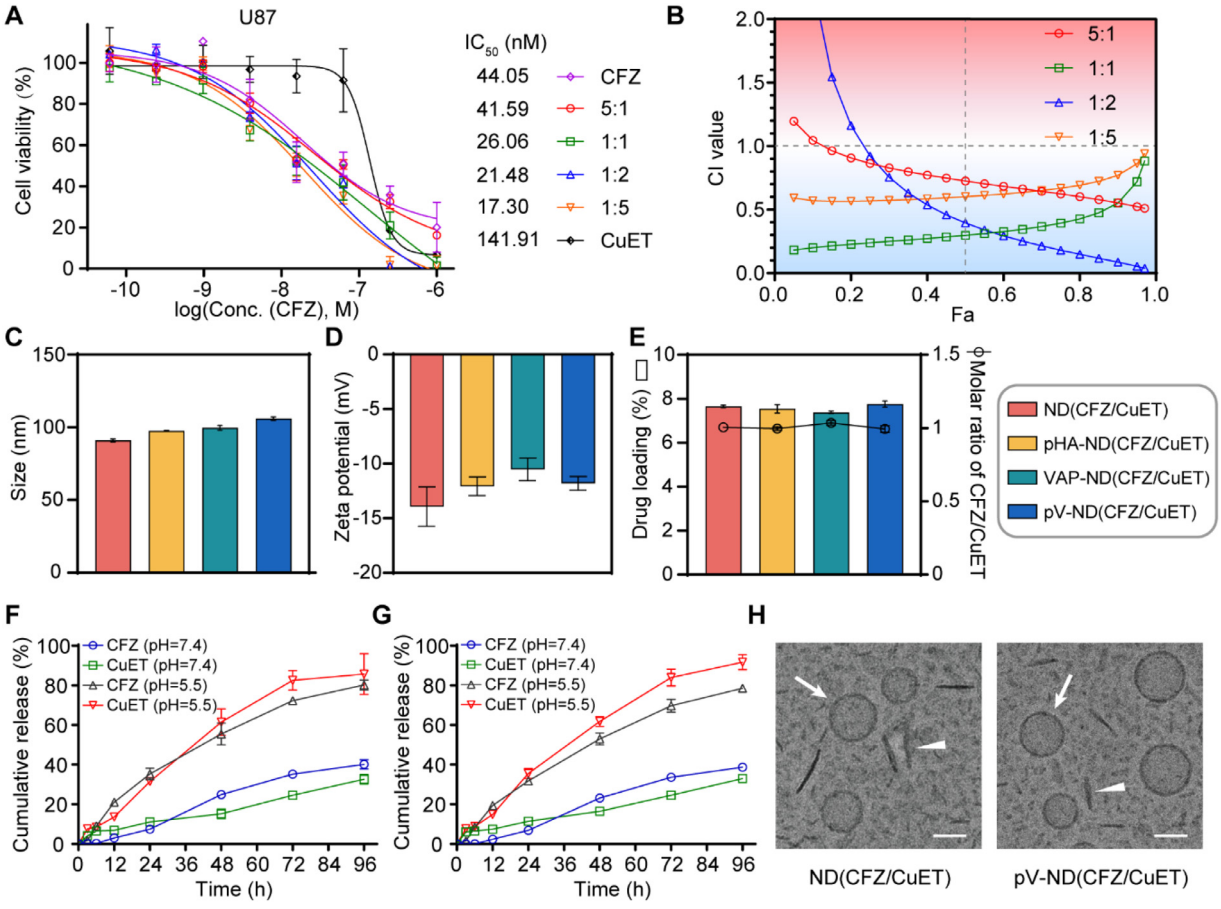

Fig. 1 – Preparation and characterization of ND(CFZ/CuET) formulations. (A) Cytotoxic effects of CFZ, CuET and CFZ/CuET mixture at different ratios on U87 cells after 72 h incubation. (B) CI values of CFZ/CuET mixture on U87 cells at different ratios. (C, D) Particle size and zeta potential of ND(CFZ/CuET), pHA-ND(CFZ/CuET), VAP-ND(CFZ/CuET) and pV-ND(CFZ/CuET). (E) Total drug loading capacity and the molar ratio of CFZ/CuET in different ND formulations. (F, G) *In vitro* release of CFZ and CuET from ND(CFZ/CuET) (F) and pV-ND(CFZ/CuET) (G) At 37 °C in pH 7.4 or 5.5. (H) Morphological images of ND(CFZ/CuET) and pV-ND(CFZ/CuET) identified by cyro-EM. The arrows and triangles indicated face-on and edge-on observation of NDs, respectively. Scale bars: 50 nm. (n = 3, mean ± SD).

that drug loaded in NDs also exhibited synergistic effects (Fig. S6). The CI values of pV-ND(CFZ/CuET) at Fa_{50} on U87 cells, SHG66 cells and HUVECs were 0.19950, 0.12628 and 0.35168, respectively. This indicated that CFZ and CuET showed an ideal synergistic effect when encapsulated together in NDs.

The ubiquitin-proteasome system could be disturbed by CFZ (binding to proteasome) and CuET (disabling the vital p97-NPL4-UFD1 signaling pathway) in different ways [13]. Nrf1, which has an inactive form of 120 kDa and an active form of 110 kDa, is a transcriptional activator of proteasomal genes. Activated Nrf1 is responsible for the "bounce-back" response that restores proteasome activity, causing drug resistance to CFZ [32,33]. Interestingly, Nrf1 activation is a p97-dependent process [13], indicating that CuET might reduce CFZ resistance by blocking the activation of Nrf1 (Scheme 1B). Western blot analysis of poly-Ub proteins and Nrf1 supported these assumptions (Fig. 2D). The poly-Ub proteins accumulated obviously upon treatment with CFZ, and a slight accumulation of poly-Ub proteins was also observed when treated with CuET (Fig. 2D). In SHG66 cells, which are naturally resistant to CFZ (Fig. S2A), Nrf1 expression was significantly enhanced and activated (110 kDa) upon CFZ treatment, while it was barely expressed in U87 cells (Fig. 2D). However, when CFZ was combined with CuET, the activated Nrf1 (110 kDa) was obviously inhibited (Fig. 2D), which demonstrates a possible mechanism for CuET to reduce CFZ resistance, thus leading to a synergistic effect. Moreover, previous studies showed that Nrf1 overexpression facilitated CSC growth [34–36], while CuET specifically inhibited CSCs [14,15]. Colony and spheroid formation assays were conducted to evaluate the self-renewal ability, which reflected the stemness of a single cell to form a colony [37,38]. As shown in Fig. 2E-F and Fig. S7A-S7B, U87 colonies and SHG66 spheroids were significantly inhibited by pV-ND(CuET) and pV-ND(CFZ/CuET), indicating that the cell stemness could be suppressed by CuET but not CFZ.

Notably, a recent study has reported a novel form of cell death named cuproptosis, which is the induction of cell death by direct binding of copper to lipoylated components in the tricarboxylic acid (TCA) cycle [16]. Since CuET is a cuproptosis inducer [16] and CFZ is a common apoptosis

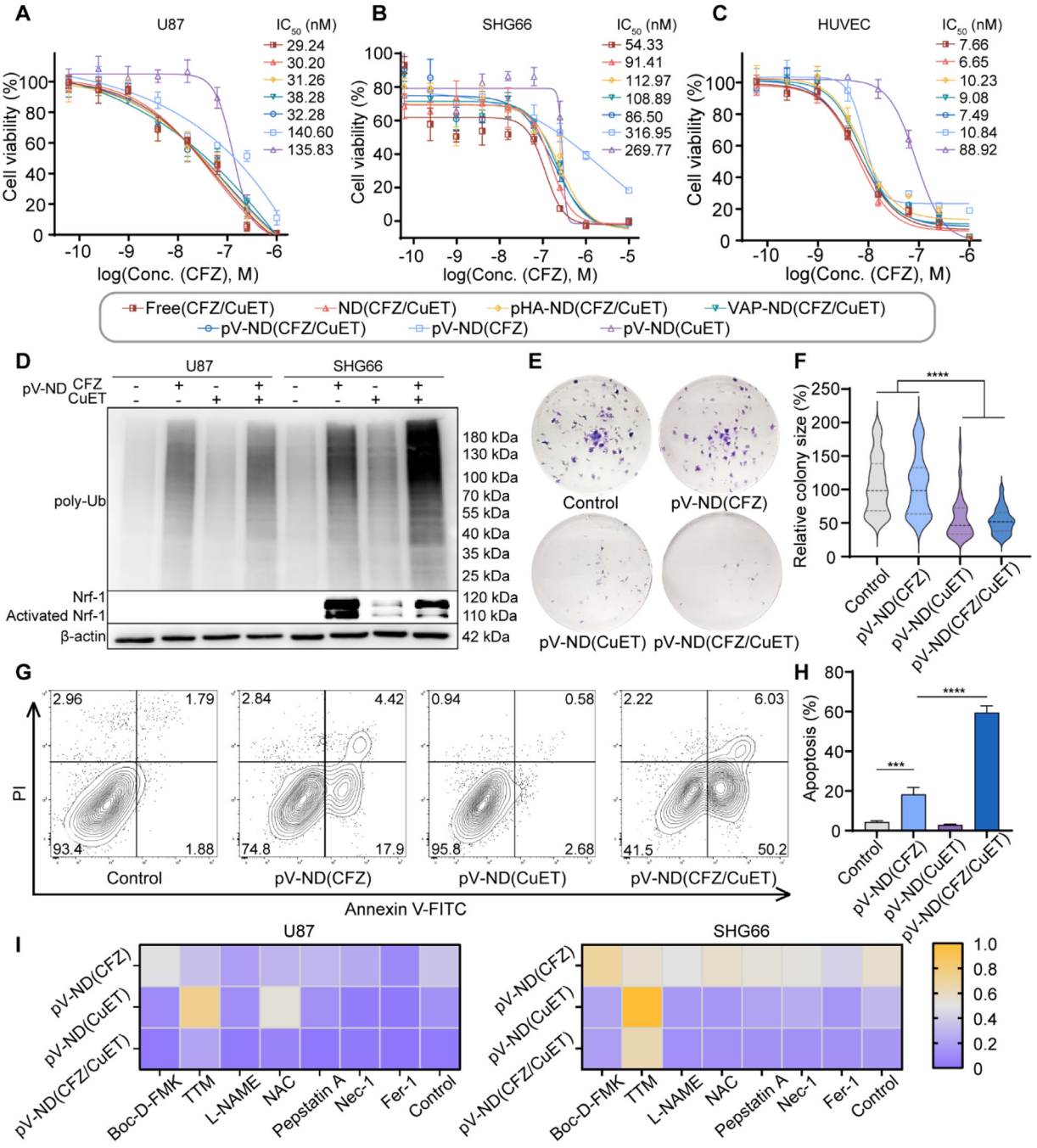

Fig. 2 – Cytotoxicity and mechanisms of pV-ND(CFZ/CuET). (A-C) Cytotoxic effects of different formulations on U87 cells, SHG66 cells and HUVECs. (D) Expression levels of poly-Ub protein and Nrf1 in U87 cells and SHG66 cells. (E, F) Colony formation assay and relative colony size of U87 cells incubated with different ND formulations. (G, H) Contour plot and apoptosis rates of U87 cells incubated with different ND formulations. (I) Heatmap of U87 cells and SHG66 cells rescued by 50 mM Boc-D-FMK, 20 mM TTM, 300 mM L-NAME, 1 mM NAC, 1 mM pepstatin A, 20 mM Nec-1 or 10 mM Fer-1 and then treated with different ND formulations for 72 h ($n = 3$, mean ± SD).

inducer [39], their combination could lead to different modes of cell death simultaneously. The apoptosis rates induced by pV-ND(CFZ/CuET) on U87 cells and SHG66 cells were about 59.4 % and 18.5 % respectively, and there was no significant apoptosis rate improvement caused by pV-ND(CuET) under experimental conditions (Fig. 2G-2H and S8A-S8B). The cuproptosis was evaluated by cell rescue experiment [16]. Treatment with inhibitors of cell death mechanisms were used to rescue cells, including apoptosis inhibitor (Boc-D-FMK), cuproptosis inhibitor (TTM), nitric oxide synthase inhibitor (L-NAME), reactive oxygen species (ROS) scavenger (NAC), aspartase inhibitors (Pepstatin A), necroptosis inhibitor

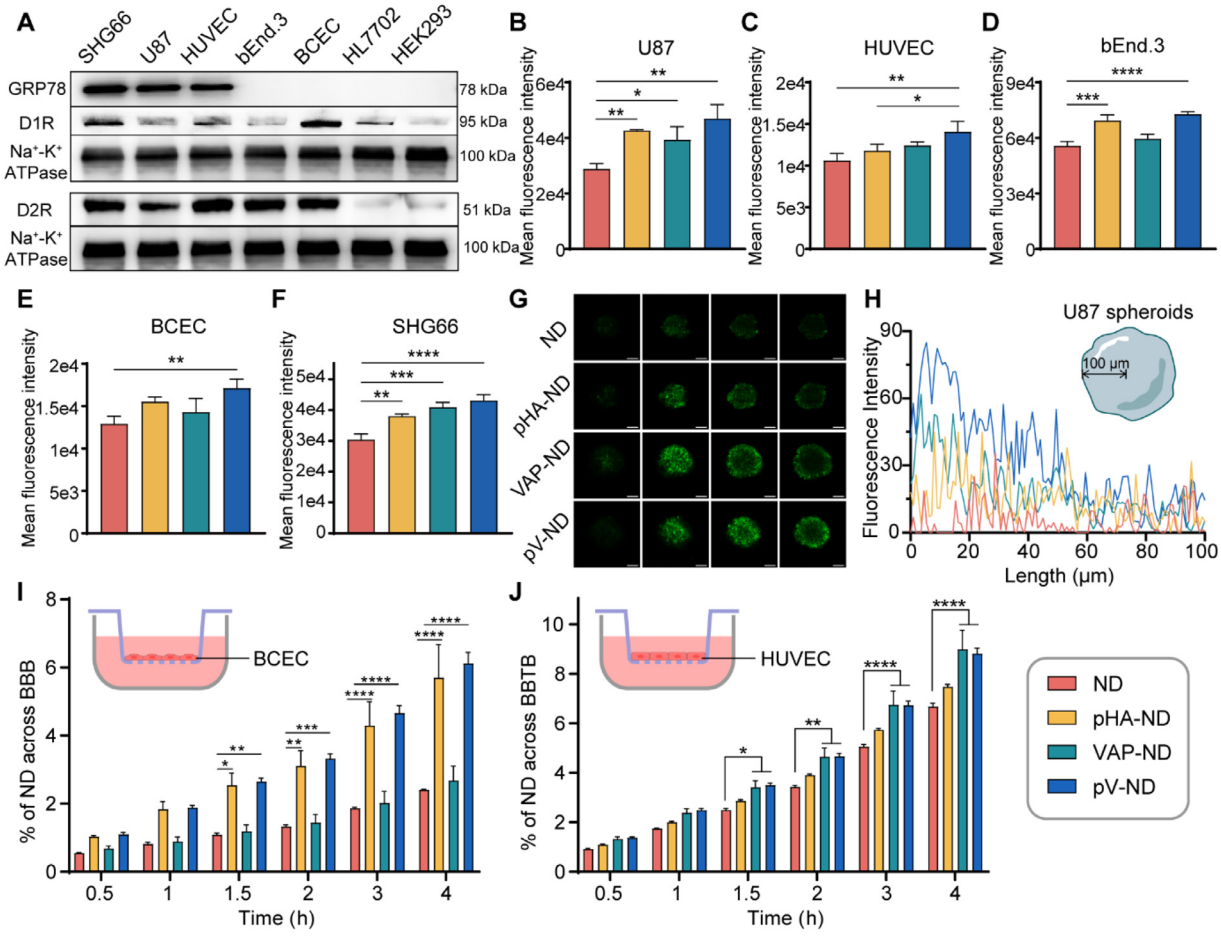

Fig. 3 – *In vitro* targeting ability of different ND formulations. (A) GRP78 and D1R protein expression on the membrane of different cell lines. (B-F) Cellular uptake after incubation with different ND formulations for 4 h by U87 cells, HUVECs, bEnd.3 cells, BCECs and SHG66 cells. (G) Penetration of different ND formulations into U87 tumor spheroids, with 25 μm intervals between each slide. Scale bars: 100 μm. (H) Quantitative analysis of NDs penetrating U87 tumor spheroids. (I, J) Schematic illustration of the *in vitro* BBB/BBTB model and transcytosis efficiency of different ND formulations in the BBB or BBTB model. ($n = 3$, mean ± SD).

(Nec-1) and ferroptosis inhibitor (Fer-1) [16]. As shown in Fig. 2I, cell death induced by pV-ND(CFZ) was reduced by Boc-D-FMK. Cell death caused by pV-ND(CuET) was remarkably rescued by TTM and slightly rescued by NAC, indicating that the effect of CuET was mainly related to cuproptosis and slightly related to oxidative stress. Taken together, these results demonstrated that pV-ND(CFZ/CuET) exerted a synergistic effect on ubiquitin-proteasome system and could induce apoptosis and cuproptosis simultaneously.

3.3. *All-stage targeting ability of pV-ND*

Since DR is the receptor of pHA and GRP78 is the receptor of VAP, we first analyzed the expression of D1R, D2R and GRP78 proteins on the cell membrane of SHG66 cells, U87 cells, HUVECs, bEnd.3 cells and BCECs (Fig. 3A), with HL7702 and HEK293 cells being the normal cell control. GRP78 proteins were highly expressed on the surface of SHG66 cells, U87 cells and HUVECs. D1R proteins were expressed at different levels in all detected cell lines, and the expression of D1R proteins in BCECs was higher than that in other cell lines. D2R proteins were highly expressed in SHG66 cells, U87 cells, HUVECs, bEnd.3 cells and BCECs. These highly expressed receptors could mediate the binding of corresponding ligands and further enhance endocytosis efficiency.

Cellular uptake of pV-ND by U87 cells, HUVECs and SHG66 cells was significantly higher than that in ND groups, indicating that pV possessed tumor targeting ability (Fig. 3B, 3C and 3F). The enhanced cellular uptake mainly came from the expression of D1R and GRP78 on the cell surface. For bEnd.3 cells and BCECs (Fig. 3 D and 3E), both pHA-ND and pV-ND were taken up more efficiently than ND and VAP-ND due to the high expression of D1R and the absence of GRP78 on the surface of bEnd.3 cells and BCECs (Fig. 3A). Confocal images of cellular uptake corroborated the above results, in which pV-ND showed a stronger uptake than other ND formulations (Fig. S9A-S9E). Tumor spheroids were cultured to mimic solid tumors that were difficult to be penetrated. For

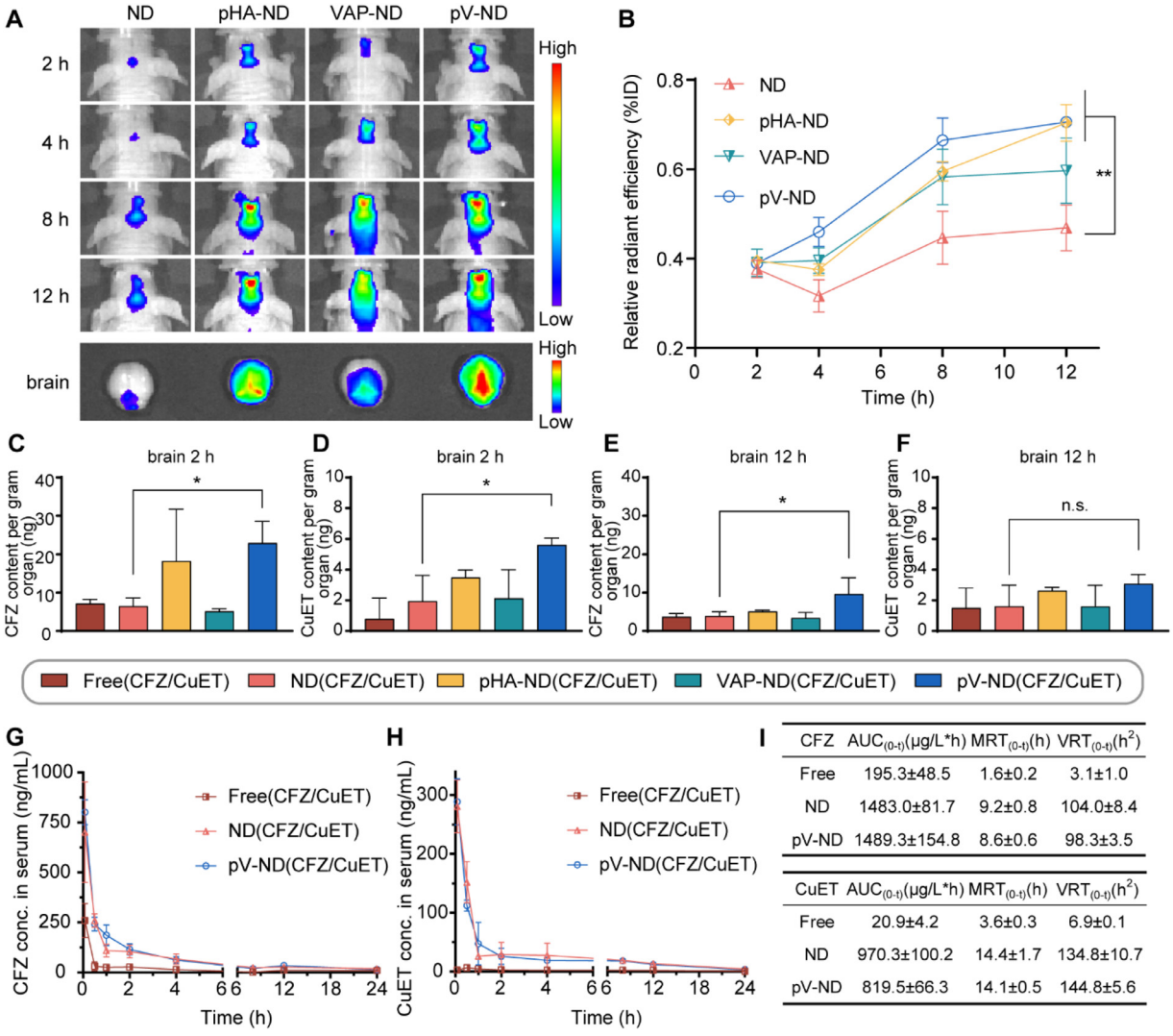

I

CFZ	$AUC_{(0-t)}$(μg/L*h)	$MRT_{(0-t)}$(h)	$VRT_{(0-t)}(h^2)$
Free	195.3±48.5	1.6±0.2	3.1±1.0
ND	1483.0±81.7	9.2±0.8	104.0±8.4
pV-ND	1489.3±154.8	8.6±0.6	98.3±3.5

CuET	$AUC_{(0-t)}$(μg/L*h)	$MRT_{(0-t)}$(h)	$VRT_{(0-t)}(h^2)$
Free	20.9±4.2	3.6±0.3	6.9±0.1
ND	970.3±100.2	14.4±1.7	134.8±10.7
pV-ND	819.5±66.3	14.1±0.5	144.8±5.6

Fig. 4 – *In vivo* biodistribution and pharmacokinetics. (A) Images of DiR-labeled ND, pHA-ND, VAP-ND and pV-ND accumulating in orthotopic U87 glioma-bearing nude mice. Mouse brains were imaged 12 h after administration. (B) Relative radiant efficiency of ND, pHA-ND, VAP-ND and pV-ND in the brains of U87 glioma-bearing nude mice. (C, D) Biodistribution of CFZ and CuET in U87 glioma-bearing nude mouse brains after 2 h administration. (E, F) Biodistribution of CFZ and CuET in U87 glioma-bearing nude mouse brains after 12 h administration. (G, H) Pharmacokinetic curves of CFZ and CuET after administration with different CFZ/CuET formulations. (I) Pharmacokinetic parameters of CFZ and CuET. (n = 3, mean ± SD).

U87 tumor spheroids, VAP-ND and pV-ND displayed stronger fluorescence signals than ND and pHA-ND (Fig. 3G-3H), which was mainly due to the expression of GRP78 on U87 cell surface.

Barrier-crossing abilities of different ND formulations in the BBB and BBTB models *in vitro* were conducted by detecting the amount of FITC-labeled NDs in the lower chambers. Both pHA-ND and pV-ND increased the BBB-crossing ability against BCEC monolayer after 4 h of incubation (2.37 and 2.54 folds when compared with ND, Fig. 3I). Both VAP-ND and pV-ND showed higher crossing ability in the BBTB model after 4 h of incubation (1.34 and 1.32 folds when compared with ND, Fig. 3J). Confocal images of the monolayer in the upper chambers of the BBB and BBTB models (Fig. S10A-S10B, S11A-S11B) were both recorded. It was observed that pV-ND showed higher fluorescence intensity in the monolayers in the BBB and BBTB models. The above results verified that the Y-shaped targeting ligand pV integrated the superiority of pHA and VAP, enabling the NDs to exhibit an all-stage targeting ability.

3.4. *In vivo targeting ability and pharmacokinetics*

The *in vivo* brain targeting ability of different ND formulations was first investigated by NIR imaging system in orthotopic U87 glioma-bearing nude mice. It was demonstrated that pV-ND showed the strongest fluorescence signal in mouse brain (Fig. 4A). In addition, the fluorescence signal of different NDs were similar in major organs (heart, liver, spleen, lung and kidney), indicating that the ligand modification did not affect the distribution in major organs (Fig. S12A). Relative radiant efficiency of pV-ND group in the brains of U87 glioma-bearing

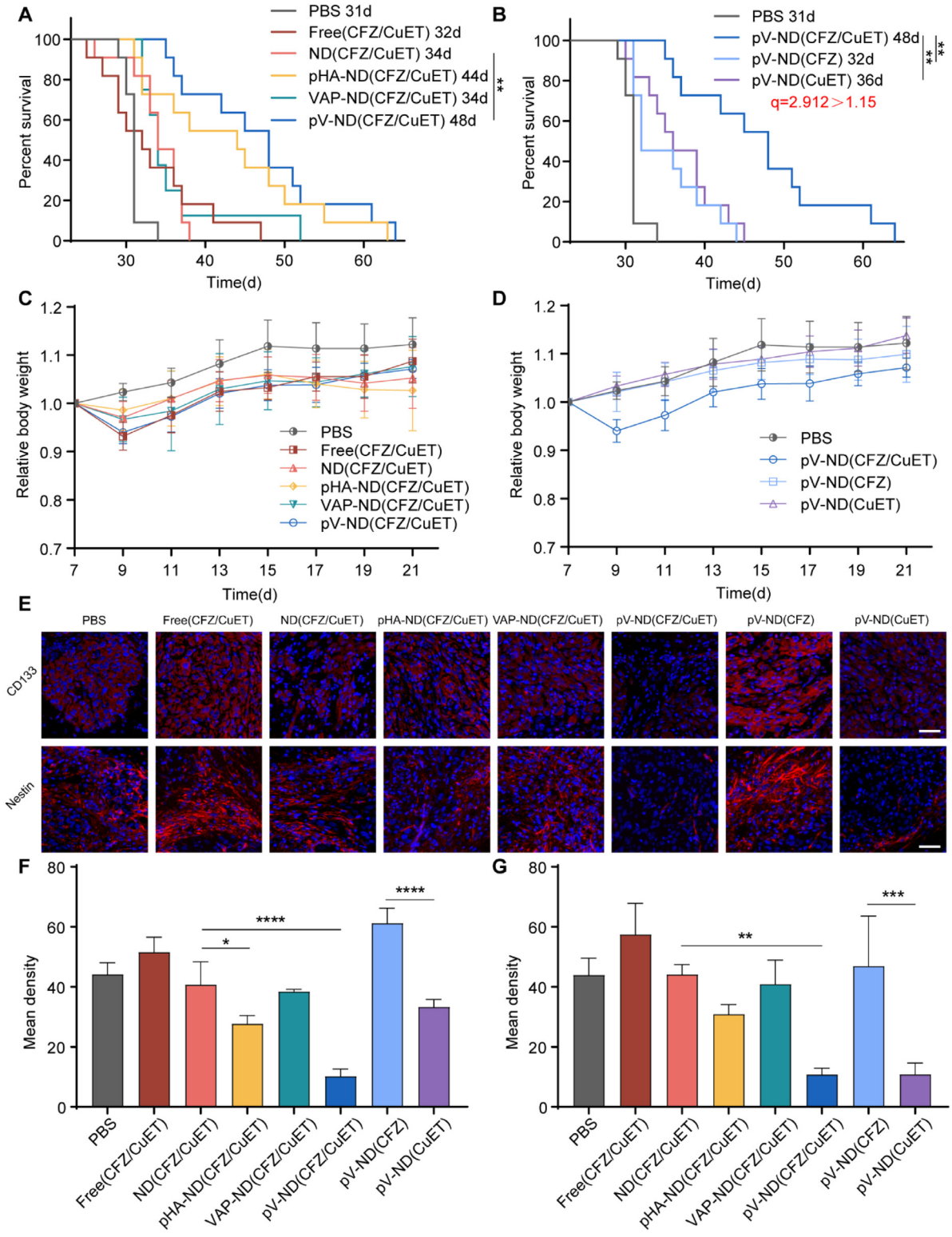

Fig. 5 – Effects of different CFZ/CuET formulations on orthotopic U87 glioma-bearing nude mice. (A) Kaplan-Meier survival curve and (C) relative body weight of glioma-bearing nude mice treated with pHA-, VAP- or pV-modified NDs. (B) Kaplan-Meier survival curve and (D) relative body weight of glioma-bearing nude mice treated with pV-NDs encapsulating CFZ, CuET or CFZ/CuET. (n = 10 or 11, mean ± SD). (E) CD133 (red) or Nestin (red) staining of brain tumor sections. The cell nuclei were stained with DAPI (blue). Scale bars: 50 μm. (F, G) Quantification of integral optical density in brain tumor sections stained by CD133 (left) or Nestin (right). (n = 3, mean ± SD).

nude mice was also significantly higher than that of ND group (Fig. 4B), indicating that pV-ND could effectively facilitate the crossing of the BBB/BBTB and accumulate in brain. We further evaluated the drug amounts of CFZ and CuET *in vivo* at 2 h and 12 h after administration. As shown in Fig. 4C-4F, the CFZ and CuET levels in the brain of glioma-bearing mice in pHA-ND(CFZ/CuET) group and pV-ND(CFZ/CuET) group were higher than those in ND(CFZ/CuET) group and Free(CFZ/CuET) group. Besides, the brain targeting of VAP-ND was not significantly improved under experimental conditions due to the early stage of glioma development and the incomplete formation of BBTB [40,41]. The amounts of CFZ and CuET in major organs (heart, liver, spleen, lung and kidney) were also analyzed and were found to be mainly distributed in the liver and spleen (Fig. S12B-S12E). These results demonstrated that the Y-shaped pV-modified NDs exhibited higher brain accumulation *in vivo* than other ND formulations.

The pharmacokinetic profiles of Free(CFZ/CuET), ND(CFZ/CuET) and pV-ND(CFZ/CuET) were analyzed by detecting the drug concentration in plasma. As shown in Fig. 4G-4H, in Free(CFZ/CuET) group, CFZ concentration declined rapidly within 0.5 h and CuET concentration was barely detectable immediately after administration. By way of contrast, both ND(CFZ/CuET) and pV-ND(CFZ/CuET) extended the blood retention of CFZ and CuET, which was reflected by the larger area under curve ($AUC_{(0-t)}$), longer mean residence time ($MRT_{(0-t)}$) and higher variance of mean residence time ($VRT_{(0-t)}$) (Fig. 4I). The pharmacokinetic behavior of ND was not affected by pV modification. Additionally, ND(CFZ/CuET) and pV-ND(CFZ/CuET) could better maintain the ratio of two drugs at a similar level when compared with Free(CFZ/CuET).

3.5. *In vivo antitumor efficacy and safety*

To evaluate the anti-glioma efficacy, the same animal model used *in vivo* targeting experiments was established. Different CFZ/CuET formulations were injected via the tail vein at the dosage of CFZ 2 mg/kg and CuET 1 mg/kg each time on Day 7, 10, 13, 16 and 19 after glioma modeling. In order to compare the therapeutic effect of different targeting ligands or different drugs, two Kaplan-Meier survival plots were generated separately, and the MST of each group was noted (Fig. 5A-5B). As shown in Fig. 5A, the MST of mice treated with pV-ND(CFZ/CuET) was significantly longer than those treated with ND(CFZ/CuET). The MST extension rates of Free(CFZ/CuET), ND(CFZ/CuET), pHA-ND(CFZ/CuET), VAP-ND(CFZ/CuET) and pV-ND(CFZ/CuET) were 3.23 %, 9.68 %, 41.94 %, 9.68 % and 54.84 % respectively, indicating that the best therapeutic efficacy was relevant to pV as the all-stage targeting ligand and ND as the drug delivery system. The Kaplan-Meier survival curve of different drugs in Fig. 5B demonstrated that co-delivery of CFZ and CuET was able to significantly prolong the survival in glioma-bearing mice. The MST extension rate of pV-ND(CFZ/CuET) (54.84 %) was higher than that of pV-ND(CFZ) group (3.23 %) and pV-ND(CuET) group (16.13 %). Furthermore, Jin Zhengjun q value was utilized to evaluate the interaction of two drugs. q value of pV-ND(CFZ/CuET) calculated against pV-ND(CFZ) and pV-ND(CuET) was 2.912 (> 1.15), indicating a strong synergistic effect of these two drugs *in vivo*. Furthermore, H&E staining of the brain sections on the day after the last administration was shown in Fig. S13. The tumor size in PBS group appeared to be the largest. Tumors from Free(CFZ/CuET), ND(CFZ/CuET), VAP-ND(CFZ/CuET) and pV-ND(CFZ) groups were similar in size and slightly smaller than that in PBS group. pV-ND(CuET) and pHA-ND(CFZ/CuET) groups showed smaller tumors, and pV-ND(CFZ/CuET) group exhibited the smallest tumor, which was basically consistent with the MSTs of each group (Fig. 5A-5B). Immunohistology experiments were conducted to analyze CD133 and Nestin level in brain tumor sections (Fig. 5E) for the quantification of glioma stem cell markers (Fig. 5F-5G). Compared with other groups, pV-ND(CFZ/CuET) remarkably reduced the expression of CD133 and Nestin, which mainly came from the anti-CSC ability of CuET.

The *in vivo* safety of ND formulations was preliminarily evaluated. Relative body weight of ND-treated mice showed no significant weight loss compared with PBS group (Fig. 5C-5D). The pV modification also showed no significant effect on body weight. Morphological changes in primary organs (heart, liver, spleen, lung and kidney) were examined by H&E staining. All the formulations showed negligible pathological changes (Fig. S14). The above results demonstrated that pV-ND(CFZ/CuET) was effective for glioma treatment, which could cross the BBB/BBTB and exert a synergistic effect with low toxicity *in vivo*.

4. Conclusion

In summary, we designed a convergent all-stage targeted strategy by the co-loading of CFZ and CuET in pV-modified NDs to conquer the biological barriers and address tumor heterogeneity. The Y-shaped targeting ligand pV endowed NDs with the BBB/BBTB-crossing ability. CFZ and CuET combination disrupted the balance of ubiquitin-proteasome system and induced cell apoptosis and cuproptosis, killing glioma cells and CSCs simultaneously. The pV-ND(CFZ/CuET) could effectively inhibit glioma development and prolong the survival in glioma-bearing mice. Additionally, we expanded the application of q value method to evaluate drug interactions *in vivo*. These findings highlight the potential of our strategy as an effective therapy for glioma and will provide a promising perspective for future drug combination research.

Conflicts of interest

The authors report no conflicts of interest. The authors alone are responsible for the content and writing of this article.

Acknowledgments

This work was sponsored by Shanghai Education Commission Major Project (2017–01–07–00–07-E00052), National Natural Science Foundation of China (No.81773657), Shanghai Sailing Program (No. 20YF1404500) and Scientific Research Foundation of Huashan Hospital, Fudan University (No. 2019QD012).

We thank the staff members (especially Jialin Duan and Lihui Xin) of the Electron Microscopy System at the National Facility for Protein Science in Shanghai (NFPS), Shanghai Advanced Research Institute, Chinese Academy of Sciences, China for providing technical support and assistance in data collection and analysis.

Supplementary materials

Supplementary material associated with this article can be found, in the online version, at doi:10.1016/j.ajps.2024.101010. The figures and tables with "S" before the serial number are included in the Supplementary material.

References

[1] Omuro A, DeAngelis LM. Glioblastoma and other malignant gliomas: a clinical review. JAMA 2013;310(17):1842–50.
[2] Tanaka S, Louis D, Curry W, Batchelor T, Dietrich J. Diagnostic and therapeutic avenues for glioblastoma: no longer a dead end? Nat Rev Clin Oncol 2013;10(1):14–26.
[3] Padmakumar S, Amiji M. Long-acting therapeutic delivery systems for the treatment of gliomas. Adv Drug Delivery Rev 2023;197:114853.
[4] van Tellingen O, Yetkin-Arik B, de Gooijer M, Wesseling P, Wurdinger T, de Vries H. Overcoming the blood-brain tumor barrier for effective glioblastoma treatment. Drug Resistance Updates 2015;19:1–12.
[5] Song B, Wang X, Qin L, Hussain S, Liang W. Brain gliomas: diagnostic and therapeutic issues and the prospects of drug-targeted nano-delivery technology. Pharmacol Res 2024;206:107308.
[6] Jain R, Stylianopoulos T. Delivering nanomedicine to solid tumors. Nat Rev Clin Oncol 2010;7(11):653–64.
[7] Bao S, Wu Q, McLendon R, Hao Y, Shi Q, Hjelmeland A, et al. Glioma stem cells promote radioresistance by preferential activation of the DNA damage response. Nature 2006;444(7120):756–60.
[8] SuvàM Tirosh I. The glioma stem cell model in the era of single-cell genomics. Cancer Cell 2020;37(5):630–6.
[9] Ludwig M, Galbraith M, Eduthan N, Hill A, Clay M, Tellez C, et al. Proteasome inhibition sensitizes liposarcoma to MDM2 inhibition with Nutlin-3 by activating the ATF4/CHOP stress response pathway. Cancer Res 2023;83(15):2543–56.
[10] Nooka A, Gleason C, Casbourne D, Lonial S. Relapsed and refractory lymphoid neoplasms and multiple myeloma with a focus on carfilzomib. Biologics 2013;7:13–32.
[11] Hawley T, Riz I, Yang W, Wakabayashi Y, Depalma L, Chang Y, et al. Identification of an ABCB1 (P-glycoprotein)-positive carfilzomib-resistant myeloma subpopulation by the pluripotent stem cell fluorescent dye CDy1. Am J Hematol 2013;88(4):265–72.
[12] Xu H, Han H, Song S, Yi N, Qian C, Qiu Y, et al. Exosome-transmitted PSMA3 and PSMA3-AS1 promote proteasome inhibitor resistance in multiple myeloma. Clin Cancer Res 2019;25(6):1923–35.
[13] Skrott Z, Mistrik M, Andersen K, Friis S, Majera D, Gursky J, et al. Alcohol-abuse drug disulfiram targets cancer via p97 segregase adaptor NPL4. Nature 2017;552(7684):194–9.
[14] Bista R, Lee D, Pepper O, Azorsa D, Arceci R, Aleem E. Disulfiram overcomes bortezomib and cytarabine resistance in down-syndrome-associated acute myeloid leukemia cells. J Exp Clin Cancer Res 2017;36(1):22.
[15] Xiao C, Li J, Wang X, Li S, Xu C, Zhang Z, et al. Hydroxyethyl starch stabilized copper-diethyldithiocarbamate nanocrystals for cancer therapy. J Controlled Release 2023;356:288–305.
[16] Tsvetkov P, Coy S, Petrova B, Dreishpoon M, Verma A, Abdusamad M, et al. Copper induces cell death by targeting lipoylated TCA cycle proteins. Science 2022;375(6586):1254–61.
[17] Dane E, Belessiotis-Richards A, Backlund C, Wang J, Hidaka K, Milling L, et al. STING agonist delivery by tumour-penetrating PEG-lipid nanodiscs primes robust anticancer immunity. Nat Mater 2022;21(6):710–20.
[18] Dai Z, Yu M, Yi X, Wu Z, Tian F, Miao Y, et al. Chain-length- and saturation-tuned mechanics of fluid nanovesicles direct tumor delivery. ACS nano 2019;13(7):7676–89.
[19] Kuai R, Yuan W, Son S, Nam J, Xu Y, Fan Y, et al. Elimination of established tumors with nanodisc-based combination chemoimmunotherapy. Sci Adv 2018;4(4):eaao1736.
[20] Wang H, Zhang Z, Guan J, Lu W, Zhan C. Unraveling GLUT-mediated transcytosis pathway of glycosylated nanodisks. Asian J Pharm Sci 2021;16(1):120–8.
[21] Sindhwani S, Syed A, Ngai J, Kingston B, Maiorino L, Rothschild J, et al. The entry of nanoparticles into solid tumours. Nat Mater 2020;19(5):566–75.
[22] Xu W, Yang S, Lu L, Xu Q, Wu S, Zhou J, et al. Influence of lung cancer model characteristics on tumor targeting behavior of nanodrugs. J Control Release 2023;354:538–53.
[23] Wu S, Lu L, Zhou J, Ran D, Wang S, Xu Q, et al. All-stage targeted therapy for glioblastoma based on lipid membrane coated cabazitaxel nanocrystals. J Controlled Release 2022;345:685–95.
[24] Ding Y, Xu Q, Chai Z, Wu S, Xu W, Wang J, et al. All-stage targeted red blood cell membrane-coated docetaxel nanocrystals for glioma treatment. J Controlled Release 2024;369:325–34.
[25] Belhadj Z, Ying M, Cao X, Hu X, Zhan C, Wei X, et al. Design of Y-shaped targeting material for liposome-based multifunctional glioblastoma-targeted drug delivery. J Controlled Release 2017;255:132–41.
[26] Wang X, Meng N, Wang S, Zhang Y, Lu L, Wang R, et al. Non-immunogenic, low-toxicity and effective glioma targeting MTI-31 liposomes. J Controlled Release 2019;316:381–92.
[27] Chou T. Preclinical *versus* clinical drug combination studies. Leuk Lymphoma 2008;49:2059–80.
[28] Chou T, Talalay P. Quantitative analysis of dose-effect relationships: the combined effects of multiple drugs or enzyme inhibitors. Adv Enzyme Regul 1984;22:27–55.
[29] Zhang Y, Zhang L, Hu Y, Jiang K, Li Z, Lin Y, et al. Cell-permeable NF-κB inhibitor-conjugated liposomes for treatment of glioma. J Control Release 2018;289:102–13.
[30] Min J, Kim J, Kim J, Kim D, Zheng Y, Park J, et al. Quantitative determination of carfilzomib in mouse plasma by liquid chromatography-tandem mass spectrometry and its application to a pharmacokinetic study. J Pharm Biomed Anal 2017;146:341–6.
[31] Jin ZJ. About the evaluation of drug combination. Acta Pharmacol Sin 2004;25(2):146–7.
[32] Weyburne E, Wilkins O, Sha Z, Williams D, Pletnev A, de Bruin G, et al. Inhibition of the proteasome β2 site sensitizes triple-negative breast cancer cells to β5 inhibitors and suppresses Nrf1 activation. Cell Chem Biol 2017;24(2):218–30.
[33] Tomlin F, Gerling-Driessen U, Liu Y, Flynn R, Vangala J, Lentz C, et al. Inhibition of NGLY1 inactivates the transcription factor Nrf1 and potentiates proteasome inhibitor cytotoxicity. ACS Cent Sci 2017;3(11):1143–55.
[34] Thompson C, MacDonald G, Mueller C. Decreased expression of BRCA1 in SK-BR-3 cells is the result of aberrant activation

of the GABP Beta promoter by an NRF-1-containing complex. Mol Cancer 2011;10:62.
[35] Zhou Y, Xu Z, Quan D, Zhang F, Zhang H, Xiao T, et al. Nuclear respiratory factor 1 promotes spheroid survival and mesenchymal transition in mammary epithelial cells. Oncogene 2018;37(47):6152–65.
[36] Bhawe K, Das J, Yoo C, Felty Q, Gong Z, Deoraj A, et al. Nuclear respiratory factor 1 transcriptomic signatures as prognostic indicators of recurring aggressive mesenchymal glioblastoma and resistance to therapy in White American females. J Cancer Res Clin Oncol 2022;148(7):1641–82.
[37] Srivastava P, Romanazzo S, Kopecky C, Nemec S, Ireland J, Molley T, et al. Defined microenvironments trigger *in vitro* gastrulation in human pluripotent stem cells. Adv Sci (Weinh) 2023;10(5):e2203614.
[38] Liu L, Vujovic A, Deshpande N, Sathe S, Anande G, Chen H, et al. The splicing factor RBM17 drives leukemic stem cell maintenance by evading nonsense-mediated decay of pro-leukemic factors. Nat Commun 2022;13(1):3833.
[39] Georgiopoulos G, Makris N, Laina A, Theodorakakou F, Briasoulis A, Trougakos I, et al. Cardiovascular toxicity of proteasome inhibitors: underlying mechanisms and management strategies. JACC CardioOncol 2023;5(1):1–21.
[40] Wang R, Zhang X, Feng K, Zeng W, Wu J, Sun D, et al. Nanotechnologies meeting natural sources: engineered lipoproteins for precise brain disease theranostics. Asian J Pharm Sci 2023;18(5):100857.
[41] Gao H. Progress and perspectives on targeting nanoparticles for brain drug delivery. Acta Pharm Sin B 2016;6(4):268–86.